



# Queueing arrival and release mechanism for K<sup>+</sup> permeation through a potassium channel

Takashi Sumikama<sup>1,2</sup> · Shigetoshi Oiki<sup>1,3</sup>

Received: 8 July 2019 / Accepted: 18 August 2019 / Published online: 27 August 2019  
© The Author(s) 2019

## Abstract

The mechanism underlying ion permeation through potassium channels still remains controversial. K<sup>+</sup> ions permeate across a narrow selectivity filter (SF) in a single file. Conventional scenarios assume that K<sup>+</sup> ions are tightly bound in the SF, and, thus, they are displaced from their energy well by ion–ion repulsion with an incoming ion. This tight coupling between entering and exiting ions has been called the “knock-on” mechanism. However, this paradigm is contradicted by experimental data measuring the water–ion flux coupling ratio, demonstrating fewer ion occupancies. Here, the results of molecular dynamics simulations of permeation through the KcsA potassium channel revealed an alternative mechanism. In the aligned ions in the SF (an ion queue), the outermost K<sup>+</sup> was readily and spontaneously released toward the extracellular space, and the affinity of the relevant ion was ~ 50 mM. Based on this low-affinity regime, a simple queueing mechanism described by loose coupling of entering and exiting ions is proposed.

**Keywords** Molecular dynamics · Single-file permeation · Knock-on · Event-oriented analysis · Queueing mechanism

## Introduction

Ion permeation through channels is a passive process simply driven by a transmembrane electrochemical potential gradient, while the permeation mechanism is a highly elaborate process involving strict ion selectivity with a rapid throughput rate [1–4]. In potassium channels, K<sup>+</sup>-selective permeation has been assumed to preferentially bind K<sup>+</sup> tightly to a selectivity filter (SF) over less permeable Na<sup>+</sup>, excluding Na<sup>+</sup> binding to the filter from the Na<sup>+</sup>-abundant extracellular solution [5–13]. However, tight K<sup>+</sup> binding hinders

rapid permeation owing to the high energy barriers to be surmounted. Thus, the “knock-on” mechanism was proposed to unite these conflicting tendencies: Upon entering a channel, a K<sup>+</sup> ion drives out other K<sup>+</sup> ions that are already tightly bound to the SF [14]. Given the crystal structure of potassium channels, the permeation mechanism is considered more geometrically constrained [15, 16]. The narrow SF does not allow passing of a permeating ion and water molecules with each other (single file), and a short SF with a limited length (12 Å) has four binding sites (S<sub>1</sub>–S<sub>4</sub>) that can hold up to four to five molecules of either ions or water molecules. Given these constraints, Morais-Cabral et al. proposed a model for K<sup>+</sup> permeation [15]. Permeating K<sup>+</sup> ions cannot occupy adjacent binding sites in the SF because of the electrostatic repulsion, and water molecules are intercalated between ions such that K<sup>+</sup> and water molecules (w) are aligned in alternating arrays, denoted as w–K<sup>+</sup>–w–K<sup>+</sup> and K<sup>+</sup>–w–K<sup>+</sup>–w. Morais-Cabral et al. considered that the interconversion between the alternating arrays yielded rapid permeation. Molecular dynamics (MD) simulations reproduced the alternating arrays, and the simulation results were interpreted as an incoming ion that forced the expulsion of the downstream ion [17–25] via the three-ion-occupied intermediate (K<sup>+</sup>–w–K<sup>+</sup>–w–K<sup>+</sup>; the “knock-on intermediate” [19]; Fig. 1, right lower snapshot) [15, 16]. This atomistic event

**Electronic supplementary material** The online version of this article (<https://doi.org/10.1007/s12576-019-00706-4>) contains supplementary material, which is available to authorized users.

✉ Shigetoshi Oiki  
oiki-fki@umin.ac.jp

<sup>1</sup> Department of Molecular Physiology and Biophysics, Faculty of Medical Sciences, University of Fukui, Fukui 910-1193, Japan

<sup>2</sup> Present Address: Nano Life Science Institute (WPI-NanoLSI), Kanazawa University, Kakuma-machi, Kanazawa 920-1192, Japan

<sup>3</sup> Present Address: Biomedical Imaging Research Center, University of Fukui, Fukui 910-1193, Japan

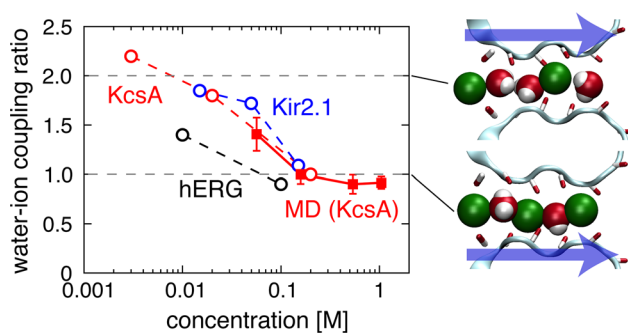


**Fig. 1** Water-ion coupling ratio ( $CR_{w-i}$ ) as a function of the  $K^+$  concentration. Experimental  $CR_{w-i}$  values as a function of  $[K^+]$ , taken from the literature, for three different potassium channels are shown: the human ether-à-go-go-Related Gene (hERG) [27], the inward rectifier (Kir2.1) [29], and the KcsA [28] channels (open circles). The concentration indicates the  $[K^+]$  on both sides of the membrane. Our simulated  $CR_{w-i}$  values are superimposed (red filled squares).  $CR_{w-i}$  increased from 1.0 with a high  $[K^+]$  to 2.0 at a low  $[K^+]$ . Snapshots on the right show typical configurations of ions (green) and water molecules (red and white) in the SF (cyan) at the transition states, where  $CR_{w-i}=2$  (upper panel) and 1 (lower panel). The arrows indicate the direction of the outward ion flux from the nanocavity side to the external side

is widely considered as a central feature of the knock-on mechanism [17–20, 26].

Despite the appealing simplicity of this mechanism, the following experimental results cast doubt on the knock-on paradigm [27–30]. In a single-file SF, permeating  $K^+$  ions and water molecules cannot move independently and ion flux is inevitably accompanied by water flux. The number of water molecules carried by one  $K^+$  ion can be counted across the single-file SF using the streaming potential [31, 32]. The water-ion flux ratio  $J_w/J_i$  [where  $J$  represents the flux for water molecule (w) and ion (i)] thus evaluated is called the water-ion coupling ratio ( $CR_{w-i}$ ) [27, 33].  $CR_{w-i}$  values of different types of potassium channels have been measured [27–29, 34, 35], and  $CR_{w-i}$  values at various  $K^+$  concentrations (Fig. 1) indicated that the knock-on mechanism is not the exclusive permeation mechanism.

In the knock-on process, the alternating array mode ( $w-K^+-w-K^+ \leftrightarrow K^+-w-K^+-w$ ) should generate a one-to-one stoichiometry, and a  $CR_{w-i}$  value of 1 was experimentally confirmed at high  $K^+$  concentrations ( $[K^+] > 0.1$  M) (Fig. 1). However, as  $[K^+]$  decreased,  $CR_{w-i}$  increased gradually from 1 toward 3, which was shared by various potassium channels including hERG, KcsA, and Kir (Fig. 1) [27–29]. The  $CR_{w-i}$  value also reflects the average number of  $K^+$  ions within the SF, having a defined number of binding sites. For example, a  $CR_{w-i}$  of 2, which has been observed at low  $[K^+]$  ( $< 0.01$  M), implies that the SF contains one or two  $K^+$  ions and the rest of the space is filled with three or two water molecules (e.g.,  $w-w-K^+-w$ ; Fig. 1, right upper snapshot). This indicates that, at low

$[K^+]$ , ions permeate not via the conventional alternating array mode but via sparse ion arrays (sparse array mode; e.g.,  $K^+-w-w-K^+ \rightarrow w-K^+-w-w \rightarrow w-w-K^+-w \rightarrow \dots$ ). The  $CR_{w-i}$  metric provides the ion and water permeation pattern in the SF, and the failure of the canonical (alternating array) mode at low  $[K^+]$  ( $< 0.01$  M) cannot be overlooked since this may threaten the present “knock-on” and “high-affinity” paradigm.

To delineate an alternative permeation mechanism, we sought to clarify the atomistic details of permeation by performing MD simulations of the KcsA potassium channel. For the KcsA channel, there have been numerous studies of the structure and function related to ion permeation [6, 7, 15–17, 20, 26, 28]. In this study, the simulation examined first whether the experimental  $CR_{w-i}$  values could be reproduced at different  $[K^+]$ . Next, the correlation of ions and water motions within the channel was analyzed using the previously developed event-oriented analysis method [36]. The analysis revealed the rates of ion arrival and release to and from the SF, from which the  $K^+$  dissociation constant of the channel was obtained. Surprisingly, we found that the  $K^+$  affinity was unexpectedly low, in contrast to the previously proposed tight  $K^+$  binding (high-affinity regime), raising questions as to the fundamental assumption about the permeation process [37]. Finally, we propose a queuing mechanism for integrating the alternating and sparse array modes, which provides a general mechanistic framework for potassium channel permeation.

## Results

### MD-simulated ion trajectories across the KcsA potassium channel

The transmembrane domain of the KcsA channel was embedded in a phosphatidylcholine membrane and exposed to various KCl concentrations (Fig. 2a). For most simulations, a positive membrane potential of + 1000 mV was applied (+ 350 mV was also applied and other potential parameters were examined; see Supplementary Table 1), which was high relative to the physiological changes in the membrane potential but relevant to experimental conditions [38–41] and previous simulations for examining permeation properties [18, 19, 36, 42–44]. The outward  $K^+$  flux was examined because physiologically, potassium channels operate under the application of an outward driving force. The root-mean-square fluctuation of  $\alpha$ -carbon atoms in the transmembrane domain was  $< 2.0$  Å [45], indicating that the channel remained in its open conformation throughout the simulation. Moreover, the distances between the  $\alpha$ -carbons of the diagonal subunits in the SF were calculated to confirm that the SF was not collapsed (Supplementary Fig. S1).

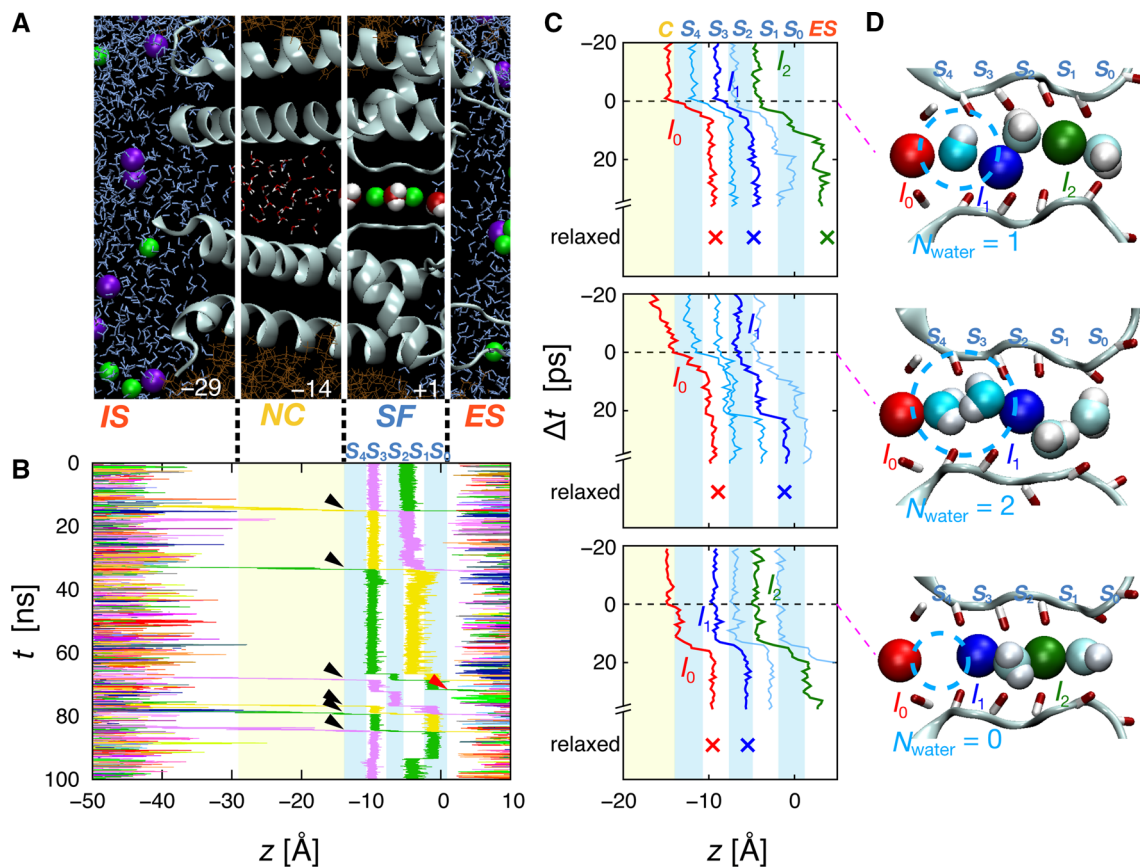


**Fig. 2** Structure of the KcsA channel and the MD-simulated ion trajectories observed at  $[K^+] = 0.15$  M. **a** The transmembrane pore domain structure of the KcsA channel (cyan ribbon) in a membrane (brown line). Residues 22–117 in two diagonal subunits are shown to illustrate the inside of the pore.  $K^+$  and  $Cl^-$  ions are denoted by green and violet spheres, respectively. Water molecules are shown with a space-filling model (the oxygen atoms are colored in dark red) in the SF, as a stick model in the NC, and as a blue line model in the bulk solution. **b** Trajectories of individual ions (varying colors) permeating through the pore ( $z$  axis) as a function of time ( $t$ ). The

black arrowheads denote SF-in events. The red arrowhead denotes spontaneous release. **c** Ion trajectories aligned to the SF-in event of  $I_0$  ( $\Delta t = 0$ ). The positions of the ions after relaxation are indicated by multi symbol. An ion ( $I_0$ ) undergoing SF-in is shown in red and the preceding ions in blue ( $I_1$ ) and green ( $I_2$ ). Water molecules intercalated upon the SF-in of  $I_0$  are shown in sky blue, and the preceding intercalated water molecules are shown light blue. **d** Snapshots of  $K^+$  and intercalated water molecules (cyan and white) as  $I_0$  undergoes SF-in. Between zero and two water molecules (marked blue circles) were intercalated

The steady open state allows a continuous ion flux without interruption.

The permeation pathway through the open pore is depicted in Fig. 2a, and a sample MD-simulated ion trajectory along the channel ( $z$  axis) is shown in Fig. 2b ( $[K^+] = 0.15$  M). Color traces, denoting individual ions, reveal the progression of ions from the intracellular space (IS) into the nanocavity (NC), followed by progression through the successive sites within the SF before being released into the extracellular space (ES).  $K^+$  ions frequently access the entrance of the NC, but only a fraction of them enter the NC. Thus, a water-filled NC is mostly empty of ions and transiently holds up to one  $K^+$  ion (digitalized occupancy) [36]. A hydrated  $K^+$  ion rapidly traverses the NC and enters the SF by shedding most of the water molecules. In the SF, ions and water molecules

progress in a single file from the  $S_4$  to the  $S_0$  site. The number of ions simultaneously occupying the SF was 1–3. During a total simulation time of 2.9  $\mu s$ , 105 ions were transferred from the IS to the ES. This is equivalent to an electric current of  $5.8 \pm 1.9$  pA, which is roughly comparable with the experimental value observed in the phosphatidylcholine membrane (the single-channel conductance of the KcsA channel in the phosphatidylcholine membrane is approximately one-sixth of that in the phosphatidylglycerol membrane [46, 47]). Concomitantly, 104 water molecules were transferred across the pore, implying  $CR_{w-i} = 0.99 \pm 0.10$ . These data are consistent with experimental measurements in various types of potassium channels exposed to high  $K^+$  concentrations (i.e.,  $[K^+] > 0.1$  M) such as KcsA, hERG,  $Ca^{2+}$ -activated  $K^+$  channel, and Kir2.1 (Fig. 1) [27–29, 35].

To examine the concentration-dependent changes in  $CR_{w-i}$ , we ran MD simulations on three additional  $K^+$  concentrations (0.05, 0.52, and 1.02 M; Supplementary Table 2). The  $CR_{w-i}$  values measured from these trajectories are plotted in Fig. 1 (filled red squares), with the previous KcsA experimental results superimposed (red open circles) [28]. These simulations provided the first reproduction of the experimental data, featuring a substantial increase in  $CR_{w-i}$  at low  $[K^+]$ , thus warranting further examination of the microscopic details of the permeation process.

### Ion and water trajectories and distributions at high $[K^+]$

We analyzed the permeation process by using the event-oriented analysis method that we developed previously [36]. In the event-oriented analysis, first, an arbitrary event occurring along the MD-simulated ion trajectories was chosen. One such event selected here was the entry of a  $K^+$  ion into the SF from the NC (Fig. 2a). Figure 2b illustrates six different SF-in events (black arrowheads in Fig. 2b), and three of the time courses were expanded in the picosecond time scale by defining the SF-in moment as the origin of the time axis ( $\Delta t = 0$ ) (Fig. 2c) [48]. In Fig. 2c, an SF-in ion is denoted as  $I_0$  (red), and two other ions, which previously underwent SF-in and remained in the SF, are denoted as  $I_1$  (blue) and  $I_2$  (green). The trajectories of the water molecules are drawn in light blue. A snapshot taken at the SF-in moment of  $I_0$  ( $\Delta t = 0$ ) (Fig. 2d, upper panel) shows that a water molecule is intercalated between  $I_0$  and  $I_1$  (shown in sky blue). Occasionally, zero or two water molecules are intercalated (Fig. 2d, lower and middle panels) [26].

The motions of  $I_0$ ,  $I_1$ , and  $I_2$  are strongly coupled [18, 19]. After the SF-in of  $I_0$ , the SF transiently holds three ions, forming the three-ion-occupied transition state. This intermediate was alleviated by an exit of the outermost  $I_2$  ion, and ensemble averaging of the SF-in event-oriented trajectories revealed that the intermediate had a brief lifetime of a hundred picoseconds. The remaining  $I_0$  and  $I_1$  then gradually shifted forward to reach sites  $S_3$  and  $S_1$ , respectively, eventually forming a “relaxation” state of about 1500 ps after the SF-in (Supplementary Fig. S2). The ion locations in the relaxation state are denoted with a “multiplication symbol” in Fig. 2c. These ion permeation processes repeat periodically and are integrated into a cyclic diagram (Fig. 3a) [36]. Three epoch-making events are depicted with approximate time intervals. Before the SF-in, an ion enters the NC, the moment of which is denoted as NC-in. After the SF-in, the ions and water molecules in the SF reach a stable occupancy state (the relaxation state), after which the ions are immobilized in their position (“frozen”) [36] until the arrival of the next ion at the NC-in moment.

The permeation process is quantitatively evaluated by analyzing the time-lapse distributions of ions and water molecules. Figure 3b shows the distribution of ions (upper panel) and water molecules (lower panel) at three defined moments in the permeation process (event-oriented distribution) at two different  $[K^+]$ . The uppermost and lowermost panels represent the distributions at two successive SF-in moments, and the middle panels show the distribution at the “relaxed” state and the next NC-in moment. The number labeling each peak represents the fractional number of the corresponding ion ( $I_0 - I_3$ ; Fig. 3b, upper panels) and the absolute number of water molecules intercalated between  $I_0$  and  $I_1$  (lower panels) at the relevant site.

At the SF-in moment at  $[K^+] = 0.15$  M (Fig. 3B, right top or bottom),  $I_1$  is predominantly located at  $S_3$  (69%) and water molecules upstream from  $I_1$  are mostly located at  $S_4$ , where the number of water molecules is 0.86. In single-file permeation, water molecules upstream of  $I_1$  are intercalated between  $I_1$  and  $I_0$  upon the SF-in of  $I_0$ . The cumulative sum of water-molecule distributions upstream from  $I_1$  at  $S_4$  and  $S_3$  is counted as  $N_{\text{water}} = 0.86 + 0.30 = 1.16$  at the SF-in moment. This number of water molecules is driven by the ion flux along the channel, leading to alternating (1:1) ion and water distributions within the SF. Thus, the microscopically observed  $N_{\text{water}}$  at the SF-in corresponds to the overall number of water and ion flux ratio during the whole simulation time ( $CR_{w-i} = 0.99$ ) as well as to the experimentally measured  $CR_{w-i}$  values (Fig. 1). Similar  $N_{\text{water}}$  values were obtained when repeating the simulations for  $[K^+] = 0.52$  and 1.02 M, being 1.1 and 1.17, respectively (Supplementary Fig. S3). Thus, the alternating array mode predominates above the  $[K^+]$  of 0.15 M.

### Spontaneous release of ions from the SF and the dissociation constant

Noticeable differences in the ion and water distributions were observed at lower  $[K^+] (= 0.05$  M) (Fig. 3b, left panel). At the SF-in, the number of water molecules located at  $S_3$  was as high as 0.86 and  $N_{\text{water}}$  was approximately 2 ( $1.78 = 0.92 + 0.86$ ), which is consistent with the experimental  $CR_{w-i}$  value. More water molecules were intercalated because  $I_1$  shifted outward such that more than half of  $I_1$  was located at  $S_2$  or  $S_1$  ( $57\% = 50\% + 7\%$ ). Why was  $I_1$  shifted further downward at low  $[K^+]$ ? We found that nearly half of  $I_2$  had already been released out to the ES (49%) before the SF-in, retaining only one  $K^+$  in the SF. In this case, permeation proceeded without passing through the three-ion-occupied knock-on intermediate, posing a question as to the prerequisite role of the transition intermediate for permeation. After the SF-in, two ions ( $I_0$  and  $I_1$ ) shifted gradually until the relaxed state, during which half of  $I_1$  was spontaneously released (Fig. 3, left “relax” panel). This spontaneous release

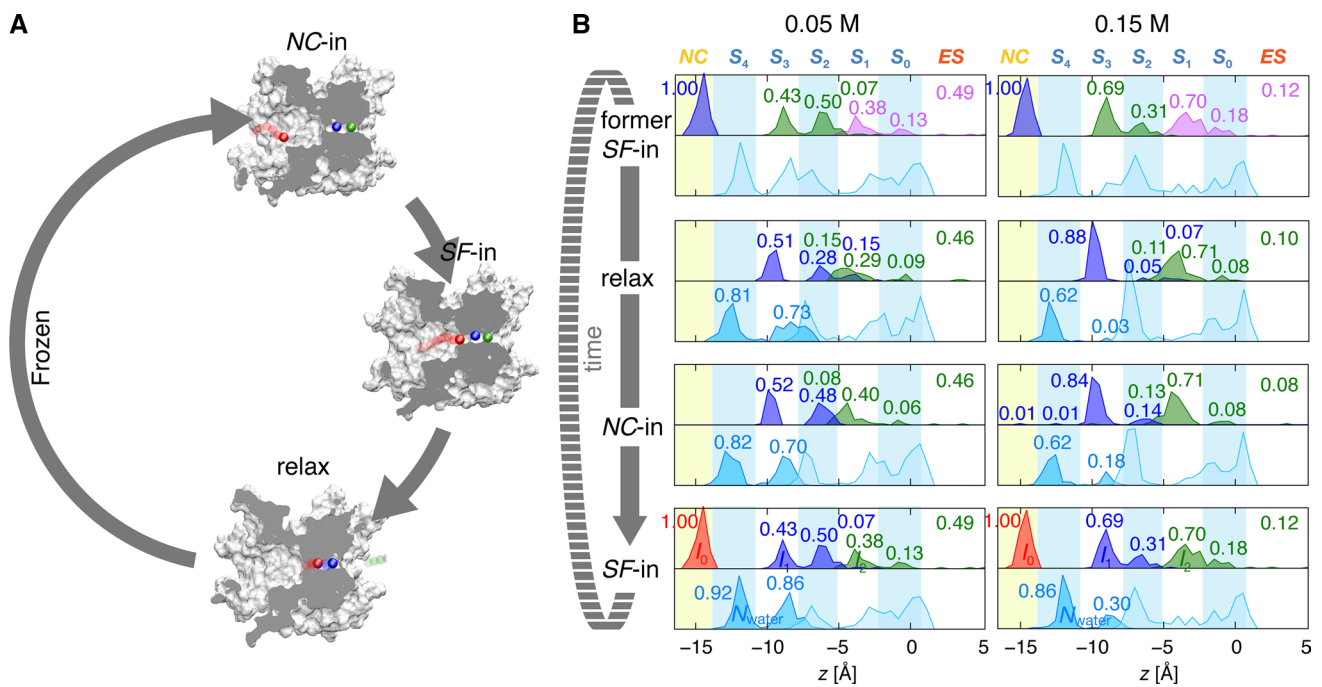


**Fig. 3** Positions of ions and water molecules during the permeation cycle. **a** A cyclic diagram for  $K^+$  permeation [36]. Among the permeation events, NC-in and SF-in events followed by relaxation are epochs for characterizing the permeation. After the relaxation, ions and water molecules are immobilized in the SF until the next NC-in (frozen period). In this cyclic diagram, two ions are bared in the SF at the NC-in moment, giving rise to the alternative array mode. Variable single-channel conductances of various potassium channels can be accounted for by the elapsed time of the frozen period governed by the entrance geometry of the NC [74]. **b** Evolution of the ion and water distributions in the SF during the permeation for  $[K^+] = 0.05$  (left panel) or  $0.15$  M (right panel). Upper panels: density distribu-

tions of  $I_0$  (red),  $I_1$  (blue),  $I_2$  (green), and  $I_3$  (the ion entering ahead of  $I_2$ ; magenta) along the  $z$  axis. Lower panels: density distributions of the water molecules, shaded in sky blue for the water molecules between  $I_0$  and  $I_1$  (i.e., upstream from  $I_1$ ), and in light blue for those downstream from  $I_1$ . For the ion distribution, the numbers beside the peaks indicate their integrals, yielding the fractional number of the corresponding ion ( $I_0$ – $I_3$ ; upper panels). For example, at  $0.15$  M  $[K^+]$ ,  $0.69$  of  $I_1$  is located at  $S_3$  and  $0.31$  is located at  $S_2$  at the SF-in moment. For the water distribution, the numbers beside the peaks indicate the absolute number of water molecules intercalated between  $I_0$  and  $I_1$  (lower panels) at a relevant site

was frequently seen in the ion trajectories at  $0.05$  M (Supplementary Fig. S4). Unexpectedly, spontaneous release was also seen even at  $0.15$  M (red arrowheads in Figs. 2b, 4a, and Supplementary Video 1),  $0.52$  M, and  $1.02$  M (Supplementary Fig. S5). At  $0.15$  M,  $12\%$  of  $I_2$  exited to the ES before the SF-in. Lower ion occupancy in the SF led to greater water molecule occupancy in the SF, which yielded a high  $CR_{w-i}$  value. The spontaneous release of  $I_2$  before the entry of  $I_0$  marks a significant departure from the conventional knock-on paradigm. Accordingly, we call this permeation as the sparse array mode, which appeared more or less in all the concentration ranges examined.

After the ion and water motions ceased (the frozen state), the distribution remained until the next NC-in moment (Fig. 3; Supplementary Fig. S3 at  $0.52$  M and  $1.02$  M) [36]. The period from the relaxed moment to the NC-in moment took up most of the permeation cycle time ( $92\%$  at  $0.15$  M), which was expressed as a long frozen period [36]. Thus, the distribution at the relaxed state represents a steady distribution of ions and water in the SF. At  $0.05$  M, the probability

of  $I_2$  occupancy in the SF decreased to  $\sim 0.5$ , indicating that the dissociation constant  $K_d$  was  $\sim 0.05$  M (see Supplementary Fig. S6). Although this affinity represents an attribute of the outermost ion in the two-ion-occupied state rather than an attribute of a specific site in the SF, this value is consistent with the experimental  $K_d$  values of  $0.009$ – $0.050$  M [30, 49–52], while a very low value of  $0.0004$  M was also reported by Lockless et al. [13]. The occupancy of the outermost ion in the SF was equilibrated with the bulk ES with a low affinity, leading to a spontaneous release. In contrast to the assumption in earlier studies that the  $K^+$  affinity for the SF should be high, the knock-on motion postulating strong ion–ion repulsion is not necessary for permeation.

### De-queueing and en-queueing rates

We show that both the alternating and the sparse array mode existed at all the concentration ranges examined. To examine the transitions between two modes, we consider the permeation as a queueing process, in which permeating ions

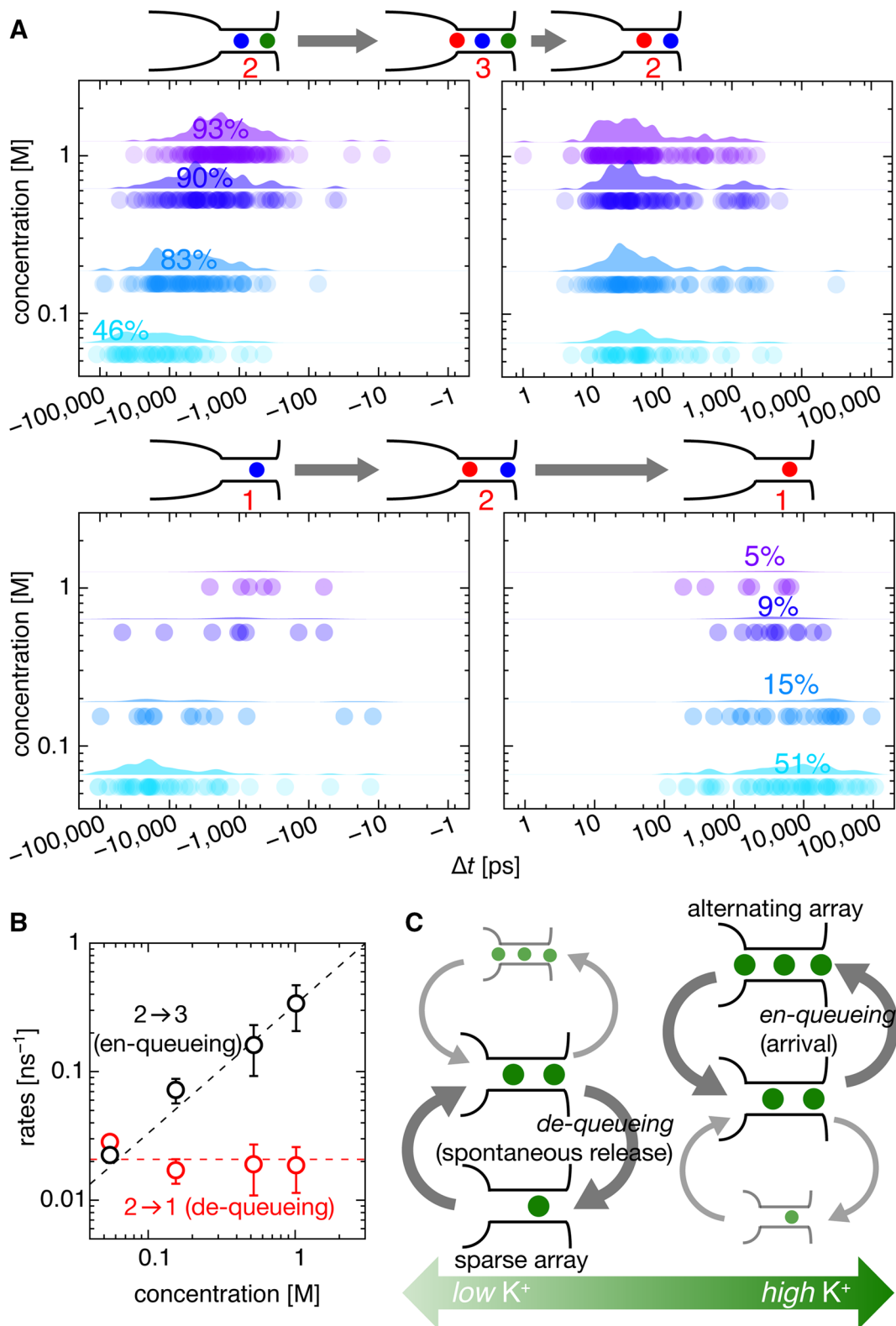


**Fig. 4** Time spent in spontaneous release, knock-on, waiting periods, and a queueing permeation model. **a** Distribution of entry times to the SF (en-queueing time; left boxes) and exit times of the outermost ion from the SF (de-queueing time; right boxes) for different  $[K^+]$ . Zero time ( $\Delta t=0$ ) is set to coincide with the SF-in for  $I_0$ . The dots represent raw data, and the distributions denote their kernel density estimation. The upper panel represents a two-ion-occupied SF before the SF-in, and the lower panel represents a

one-ion-occupied SF. **b** Rates from the two-ion-occupied state to the one- (red) and three-ion-occupied (black) states. The black dashed line represents a linear fit for the data ( $\text{rate}=[K^+]\cdot 0.33 \text{ ns}^{-1}$ ), and the red dashed line is a fit calculated from a constant ( $0.021 \text{ ns}^{-1}$ ). **c** The queueing model. The ions in the SF are shown by green circles. During the long-elapsed time frame for spontaneous release, two water molecules follow and are then intercalated between ions upon the next SF-in, which is measured as  $CR_{w-1}=2$

are in a waiting line to be processed [53, 54]. The exit of the outermost ion into the ES (release) is expressed as de-queueing and the arrival of an incoming ion into the SF (arrival) is en-queueing. When de-queueing, or spontaneous release, occurs earlier than en-queueing, the sparse array mode proceeds. When the sequence of events is reversed, the alternating array mode proceeds. Such considerations of the queueing process provide further quantitative evaluation for the permeation mechanism.

In the alternating array mode, a third ion enters the SF while with two ions in the SF (en-queueing,  $2 \rightarrow 3$ , where the number shows that of ions in the SF hereinafter; Fig. 4a, left upper panel) and then the outermost ion exits (de-queueing,  $3 \rightarrow 2$ ; Fig. 4a, right upper panel). The transition of  $2 \rightarrow 3$  occurs after a long waiting period [36]. Then,  $3 \rightarrow 2$  represents the “knock-on” process, constituting a permeation cycle of  $2 \rightarrow 3 \rightarrow 2$ . In the sparse array mode, one of two ions in the SF spontaneously exits to the ES, leaving only one ion in the SF (de-queueing,  $2 \rightarrow 1$ ; Fig. 4a, right lower panel). Then, a second ion enters the SF (en-queueing,  $1 \rightarrow 2$ ; Fig. 4a, left lower panel), constituting a  $2 \rightarrow 1 \rightarrow 2$  permeation cycle. Accordingly, it is critically important to know which of the transitions from the two-ion-occupied state happens earlier to either de-queueing or en-queueing.

Now, a quantitative evaluation of the MD-simulated trajectories was performed. First, the exit (de-queueing) time was quantified (Fig. 4a, right panels). Upon the SF-in, the SF holds either two ( $I_1$  and  $I_2$ , upper panel) or one ( $I_1$ , lower panel) ion, and an event-oriented analysis was performed for these two separate cases at different  $[K^+]$ . From the collection of the trajectories, the elapsed time from the SF-in to the release of either  $I_2$  (upper panel) or  $I_1$  (lower panel) was plotted as dots (Fig. 4a; all the data are shown in Supplementary Fig. S7). The distribution chart above the dots shows the kernel density estimation, deduced from the elapsed time, giving a coarse approximation of the probability density function for the de-queueing time (see “Materials and methods”).  $I_2$  typically exited the channel within 100 ps of  $I_0$  entering the SF ( $3 \rightarrow 2$ : upper right panel), and this de-queueing time is invariable for different concentrations. This immediate alleviation from the transient three-ion-occupied intermediate was expected to be a knock-on scenario, while the time course was first elucidated in this simulation. Another type of de-queueing is spontaneous release ( $2 \rightarrow 1$ : lower right panel), which is significant here for the sparse array mode to proceed. This de-queueing occurs long after the en-queueing (SF-in), with an elapsed time of 16,000 ps at 0.05 M, which is in dramatic contrast with the de-queueing time for the  $3 \rightarrow 2$  transition. Hence, such long-overdue time for de-queueing is poorly expressed as the coupling between en-queueing and de-queueing, and the exit process of  $2 \rightarrow 1$  is accordingly called the spontaneous release process. During

the period of spontaneous release,  $I_0$  advances deeper and more water molecules follow, providing higher  $N_{\text{water}}$  or  $CR_{w-i}$  values. This mode is frequently seen at the lower concentration of 0.05 M, occurring as high as in half of the cases (51%). Even at high concentrations, the sparse array mode was observed, though infrequently (5% at 1 M).

Next, the arrival (en-queueing) time was considered (left panels). The en-queueing occurred upon the SF-in event, and, thus, the en-queueing time could be read with the elapsed time from the less ion-occupied state to the SF-in, which is shown as dots and as the kernel density estimation ( $2 \rightarrow 3$ : upper panel;  $1 \rightarrow 2$ : lower panel). The average time for en-queueing of  $2 \rightarrow 3$  (upper left panel) gradually prolonged as  $[K^+]$  decreased. The average en-queueing time was 2800 ps for 1 M and increased to 24,200 ps for 0.05 M. This period involves a long waiting (or “frozen” [36]) period as well as the ion passage time across the NC; the values correlated well with the average permeation time at different  $[K^+]$  (3700 ns at 1.0 M and 64,500 ns at 0.05 M), which are the inverse of the current amplitudes. The en-queueing times for  $1 \rightarrow 2$  seemed to be similar to those for  $2 \rightarrow 3$  because the arrival time of the ion at the SF was independent of whether the SF occupied either one or two ions.

### Permeation through the queueing process

Now that the elapsed time for the en-queueing and de-queueing had been evaluated, the dwell time of the two-ion-occupied state can be evaluated. The time from the initiation of the two-ion-occupied state to the three- (en-queueing) or one-ion (de-queueing) occupied state depicts the dwell time of the two-ion-occupied state ( $\tau_2$ ). The value of  $\tau_2$  was 11,100 ps at 0.15 M and 19,700 ps at 0.05 M. According to the probability theory,  $\tau_2$  is independent of whether the next transition reaches either the three- or the one-ion-occupied state, while examining branching transitions ( $2 \rightarrow 3$  vs.  $2 \rightarrow 1$ ) provides a relative preference for a destination state. Figure 4a shows that, at 1.02 M, 93% of the transitions reached the three-ion-occupied intermediate ( $2 \rightarrow 3$ ; upper panel) and only 5% reached the one-ion-occupied state ( $2 \rightarrow 1$ ; lower right panel). In contrast, at 0.05 M, only 46% exhibited the  $2 \rightarrow 3$  transition and 51% of the transitions reached the one-ion-occupied state. Three parameters involving  $\tau_2$ , the separate transition rates ( $k_{23}$ ,  $2 \rightarrow 3$  en-queueing rate;  $k_{21}$ ,  $2 \rightarrow 1$  de-queueing rate), and the relative preference are related as follows (Fig. 4c):

$$\tau_2 = \frac{1}{k_{21} + k_{23}} = \frac{1}{k_{21}(1 + N_{23}/N_{21})}, \quad (1)$$

where  $N_{21}$  and  $N_{23}$  are the observed number of transitions for  $2 \rightarrow 1$  and for  $2 \rightarrow 3$ , respectively, and a relation ( $N_{23}/N_{21} = k_{23}/k_{21}$ ) was used. Accordingly, the separate transition rates of  $k_{23}$  and  $k_{21}$  were obtained by counting  $N_{23}/N_{21}$

(Fig. 4b). For example, at 0.15 M, the  $N_{23}/N_{21}$  ratio was 4.2 and  $k_{21}$  was  $0.017 \text{ ns}^{-1}$ .

Now, the en-queueing rate ( $k_{23}$ ,  $2 \rightarrow 3$ ) and the de-queueing rate ( $k_{21}$ ,  $2 \rightarrow 1$ ) were compared (Fig. 4b). The de-queueing rate (red) was nearly constant, while the en-queueing rate (black) was proportional to the concentration. Accordingly, as  $[\text{K}^+]$  decreased, the en-queueing rate decelerated until the de-queueing rate overwhelmed the en-queueing rate and the sparse array mode predominated. Thus, the two apparent modes of alternating and sparse arrays reflect the relative rates of en-queueing and de-queueing (Fig. 4c).

Lastly, the  $K_d$  value for the two-ion-occupied state was also estimated by these two rates. At the dissociation constant, the en-queueing rate was equal to the de-queueing rate (Fig. 4b). Thus, a ratio,  $k_{21}/k_{23}$ , gives the  $K_d$  value, which was evaluated to be  $\sim 0.06 \text{ M}$ . Therefore, the low  $\text{K}^+$  affinity was confirmed.

## Discussion

In this study, using the molecular dynamics (MD) simulation applied to the KcsA potassium channel, we revealed a sparse array permeation mode. With the previously established alternating array mode, the permeation processes were integrated into the queueing mechanism under the low-affinity  $\text{K}^+$  regime. The ion permeation process is dynamic in its nature, and the experimental  $CR_{w-i}$  values measured under steady-state permeation [27–29, 34, 35], rather than as equilibrium binding data, were used as a benchmark. The transport of water molecules provides crucial insights into the permeation process given the limited length of the SF with a single-file geometry. Our event-oriented analyses of ion and water-molecule trajectories illustrate the underlying atomistic events resulting from the ion-water coupling, which contradicts the conventional knock-on mechanism.

The permeation process is governed by the following principles: (i) the affinity of the outermost ion in the SF is low, and, thus, dynamic equilibrium with respect to the ES governs the occupancy of that ion (Fig. 3b); (ii) the de-queueing rate is constant, but the en-queueing rate linearly depends on  $[\text{K}^+]$  (Fig. 4b); (iii) when the spontaneous release (de-queueing) rate exceeds the arrival (en-queueing) rate, the sparse array mode appears, whereas the alternating array mode emerges when the arrival rate is faster than the release rate (Fig. 4b, c); (iv) both the alternating and the sparse mode coexist throughout all the concentration ranges (0.05–1.02 M), and the emergence of either case is stochastic (Fig. 4c). Accordingly, the ion permeation is governed by the queueing process [53, 54].

Under the framework of the general queueing theory [53, 54], permeation through the KcsA channel can be expressed as a queue waiting for service or permeation. The queue length is limited up to three  $\text{K}^+$  ions (with intercalated water

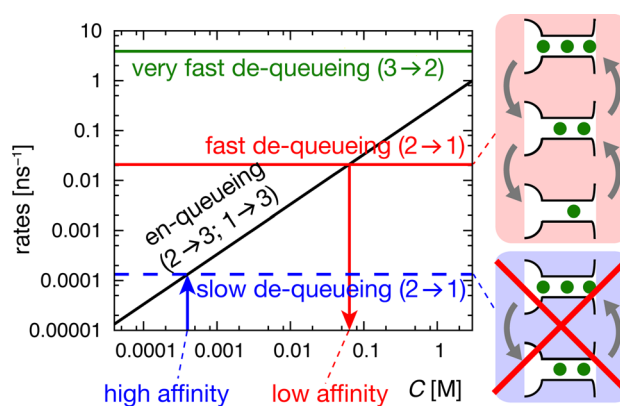


**Fig. 5** Graphical representation of the queueing mechanism with comparison to the conventional knock-on mechanism. The concentration-dependent en-queueing rate (black line) and the concentration-independent de-queueing rate ( $2 \rightarrow 1$ ; red line) are depicted from Fig. 4b. From the intersection of two lines, the  $\text{K}^+$  affinity was deduced (red arrow). The  $3 \rightarrow 2$  de-queueing rate is also shown as a green line deduced from Fig. 4a. Given the low  $\text{K}^+$  affinity, the transition from the two-ion-occupied state occurs as either en-queueing or de-queueing in a probabilistic manner. This is the queueing mechanism under the low-affinity regime (right upper cartoon). In contrast, the conventional knock-on mechanism assumes a high-affinity regime. For example, if the  $K_d$  value is  $0.0004 \text{ M}$  (blue arrow), then the de-queueing rate can be deduced (blue broken line). Then, the  $2 \rightarrow 1$  de-queueing process never occurs in the physiological concentration range, and the exclusive alternating mode or knock-on mode is allowed (right lower cartoon)

molecules) because of the geometrical length limit. At low  $[\text{K}^+]$ , ion arrival is infrequent and queueing processing in the SF (or de-queueing) is rapid (relative to arrival) enough to maintain a short queue. As the frequency of arrival ions increases, a fraction of arriving ions are not allowed to enter the channel because of the limited queue capacity. When the queue elongates up to three ions, the processing rate of the queue is accelerated.

To characterize the queueing mechanism in comparison to the conventional knock-on mechanism, we expanded Fig. 4 to include wider concentration and the rate ranges (Fig. 5), and depicted the en-queueing and de-queueing rates for the other transitions ( $3 \rightarrow 2$ ). The en-queueing rate was linear to the  $\text{K}^+$  concentration, whereas the de-queueing rate was constant. In this study, we found that the de-queueing rate of  $2 \rightarrow 1$  was high (red line) and the affinity of  $\text{K}^+$  was deduced as  $0.05 \text{ M}$  at the intersection of the en-queueing and de-queueing rates. This value is consistent with the experimental values ( $0.009$ – $0.050 \text{ M}$ ) [30, 49–52, 55]. At  $[\text{K}^+]$  below the  $K_d$  value, de-queueing ( $2 \rightarrow 1$ ) occurs earlier than en-queueing, which occurs long afterward ( $1 \rightarrow 2$ ), giving rise to the sparse array mode. At  $[\text{K}^+]$  above the  $K_d$  value, en-queueing precedes de-queueing. Once en-queueing ( $2 \rightarrow 3$ ) occurs, it immediately de-queues ( $3 \rightarrow 2$ ), yielding the predominant alternative array mode. Here, the rate of  $3 \rightarrow 2$



deduced from Fig. 4a is shown (green line). Even though the en-queueing rate and the de-queueing rate intersect at above 1 M, it does not represent the affinity of the outermost ion because the three-ion-occupied state is transient and does not give an equilibrium constant. Still, the outermost ion in the three-ion-occupied state readily exits. According to the graph, the transition of either  $2 \rightarrow 1$  or  $2 \rightarrow 3$  bifurcates into the sparse or alternate mode in a concentration-dependent and probabilistic manner (Fig. 5, right upper cartoon).

In contrast, as stated by the knock-on hypothesis, high-affinity  $K^+$  binding ( $< 0.001$  M) is implicitly assumed to be much below the physiological extracellular  $[K^+]$  (0.003–0.005 M), from which the de-queueing rate is estimated as the intersection with the en-queueing rate (blue arrow; Fig. 5). In this case, the de-queueing rate should be very slow (blue broken line), and spontaneous release cannot be expected. Thus, acceleration by an incoming ion is considered as a prerequisite for surmounting the high energy barrier from the high-affinity site. This leads to an exclusive alternating array mode, yielding a constant  $CR_{w-i}$  value of 1 over the concentration range, although it is contradictory to the experimental data.

Stoichiometry of ion and water binding to the channel being nearly one to one has been reported, though it has not been performed at lower  $[K^+]$ . In an MD simulation of the KcsA channel, Bernèche and Roux reported that ions and water molecules stably reside in the SF in an alternate array at zero membrane potential [56], indicating a  $CR_{w-i}$  value of 1. Jensen et al. also showed that  $CR_{w-i}$  was  $\sim 0.9$  for Kv1.2 and  $\sim 0.5$  for Kv1.2/2.1 [19, 44]. On the other hand, Köpfer et al. [26] reported that  $CR_{w-i}$  was 0 (no water permeation), using the same potential and channel species as the ones we used, although the driving force was imposed by the concentration gradient. A recent paper by Kopec et al. showed that the  $CR_{w-i}$  value through the MthK channel was also 0 at 220–280 mV, and was  $\sim 0.1$  at  $\sim 900$  mV [57]. On the basis of 2D-IR spectral data, however, Kratochvil et al. ruled out adjacent occupancy of ions in the SF [20]. These issues are open for further studies in the future.

The spontaneous release has been overlooked or masked because most simulations have been performed at high  $K^+$  concentrations [17, 18]. It is noteworthy that spontaneous release was observed in a previous study, although not mentioned in the relevant paper [44]. Ion permeation through the Kv1.2/2.1 channel using the CHARMM potential (we employed the AMBER force field) demonstrated the spontaneous release process when the ion parameter of Bernèche and Roux was employed. The number of ions in the channel (Fig. 2d in Ref. [44]) was below 2 (denoted as “weak  $K^+-O$ ” in the paper; voltage  $< 200$  mV), which implicates the presence of the spontaneous release process (de-queueing or  $2 \rightarrow 1$  transition). A close inspection of the free energy surface (right panel of Fig. 3c in Ref. [44]) further confirms

the presence of the spontaneous release process: there exist a basin at the two-ion center at  $-16$  Å (meaning that there is one ion in the SF) and a leaving ion at  $10$  Å (meaning that it is located in the ES), indicating that, before an incoming ion reaches the SF, one of the two ions in the SF has already flowed out to the bulk. Thus, the spontaneous release process is likely to be general in potassium channels under simulations irrespective of the choices of parameters.

One may think that spontaneous release is driven by membrane potential. However, that is not considered to be the case. Although a high transmembrane voltage, such as the 1000 mV applied in our simulations, serves as a strong driving force for rapid permeation, the spontaneous release process was observed even at weaker voltages such as 350 mV and at 1.02 M (Supplementary Fig. S5), where spontaneous releases rarely occur (as noted above, in Ref. [44], it was seen at  $< 200$  mV). At 350 mV, the ions sometimes permeate without intervening water molecules (Table S1), and this behavior is consistent with the observation in a recent paper in the case of the MthK channel [57]. Experimentally, the  $K_d$  values have been obtained exclusively at 0 mV (0.009–0.050 M) [30, 49, 50]. On the other hand, our estimated  $K_d$  value (0.05 M) was obtained at 1000 mV, which corresponds to the upper limit or within several times that of the experimental values. This means that the voltage has very little effect on the rate of the  $2 \rightarrow 1$  transition. Consequently, the membrane potential is unlikely to be the principal driving force for spontaneous ion release.

The  $K_d$  value assigned to the outermost ion in the SF is above the physiological extracellular  $K^+$  concentration (0.003–0.005 M), and, thus, the occupancy of the relevant ion should be low. Accordingly, under a physiological concentration gradient of  $[K^+]$  across the membrane, more fractions ( $> 15\%$ ) of permeation should occur via the sparse mode.

Our analysis of ion permeation and the proposed queueing permeation mechanism raise a question about the arguments for the mechanisms underlying potassium channel ion selectivity by suggesting that the conventional assumption of a high  $K^+$  affinity [5–7] is invalid. Future studies should address the interaction processes involving  $Na^+$  in the SF after binding, which underlies ion selectivity.

## Methods

### System preparation

The system at  $[K^+] = 0.15$  M was composed of one KcsA channel, 119 dioleoylphosphatidylcholine (DOPC) lipids, 30  $K^+$ , 22  $Cl^-$ , and 10,520 water molecules. First, the DOPC

bilayer was equilibrated with the surrounding KCl solution for 10 ns. MD simulation was performed using the NPT ensemble (1 bar, 310 K) with a Berendsen's barostat [58]. The area per lipid after equilibrium was confirmed to be the same as previously reported [59]. The DOPC and the solution overlapping with the pore domain (residues 22–125) of the KcsA channel and the X-ray structure (PDB code: 1K4C) [15] with F125 added to the C-terminal end were removed to incorporate the channel. E71 was protonated as in the previous study [17]. H25, E118, E120, and H124 were also protonated to adapt to the structure in the open state under acidic conditions (pH 4.0). The detailed method for making the open structure has been described previously [45]. The resultant open structure was compared with the atomic force microscopy measurements [60, 61]. An equilibrium simulation was performed for 10 ns using the NPT ensemble (1 bar, 310 K) in which  $\alpha$ -carbons were under the influence of a weak harmonic constraint [0.25 kcal/(mol Å<sup>2</sup>)]. Simulation of the equilibration using the NVT ensemble (310 K) with a Berendsen's thermostat [58] continued for 10 ns after the constraint on the KcsA channel was removed. To make the initial configuration at different concentrations, we randomly chose the water molecules and replaced them with K<sup>+</sup> and Cl<sup>-</sup>; the system was then equilibrated.

## Molecular dynamics simulations

The following empirical potentials were used: the TIP3P model for water, ff94 force field for the channel, Dang model for the K<sup>+</sup> ions, and Siu model for the lipids [59, 62–64]. The SPC/E model for water and the ff99SB force field for the KcsA channel were also examined (see Table S1) [65, 66]. Ten or 50 independent initial coordinates were generated to minimize the dependency of the initial configurations and evolved over time according to Newton's equations of motion. Several types of ion and water array in the SF (K<sup>+</sup>-w-K<sup>+</sup>-w, w-K<sup>+</sup>-w-K<sup>+</sup>, K<sup>+</sup>-w-w-K<sup>+</sup>, and K<sup>+</sup>-V-K<sup>+</sup>-w, where V stands for vacancy) were generated as initial configurations. The initial equilibrium runs, including the ion and water molecule permeation events in the process, were omitted from the analyses.

MD simulations were performed at a constant volume (78.0 × 81.2 × 85.0 Å<sup>3</sup>) and a constant temperature (310 K) using the Berendsen's thermostat [58]. Periodic boundary conditions were imposed. Long-range interactions were calculated using the particle-mesh Ewald method [67] with an 8-Å real-space cut-off. The bonds, including those for the H atoms, were constrained using the SHAKE algorithm [68] to enable a time step of 2 fs.

The SANDER module of the AMBER11 package was modified to apply an electric field and was used to observe

passive ion transport [69]. The electric field was applied to mimic a voltage-clamp experiment [70]. A voltage of 800 mV was applied to the SF (14 Å) and 200 mV was applied to the NC + IS (19 Å = 15 Å in the NC + 4 Å in the IS) (Fig. 2a) [71]. MD simulations were performed over 130 ns for 10 configurations and over 40 ns for 40 configurations, where [K<sup>+</sup>] = 0.15 M.

The SF-in moments were defined as the moment when an ion in the NC entered the SF and reached S<sub>4</sub> [36]. Similarly, the NC-in moments were defined as the moment when an ion in the IS entered the NC. Additionally, the probability of finding an ion at each site was calculated using the same method that was applied in Ref. [36].

## Kernel density estimation

To estimate the probability density of the de-queueing and en-queueing time, we used the kernel density estimation [72]. As the kernel function, a Gaussian function was used:

$$f(\Delta t) = \frac{1}{nh} \sum_{i=2}^n \frac{1}{\sqrt{nh}} e^{-(\Delta t - \Delta t_i)^2 / h},$$

where  $f$ ,  $h$ ,  $n$ , and  $\Delta t_i$  are an unknown density, a smoothing parameter called bandwidth, the quantity of the data, and each data point (shown by dots in Fig. 4a), respectively. For the value of  $h$ ,  $1/n$  was employed.

## Snapshots and videos

All snapshots and videos were produced using the Visual Molecular Dynamics package [73].

**Acknowledgements** The simulations were performed on supercomputers at the Research Center for Computational Science in Okazaki, Japan. This work was partially supported by a Grant-in-Aid for Young Scientists (no. 17K17768) to T.S. and by JSPS KAKENHI (nos. 16H00759, 16K15179, and 17H04017) to S.O. We would like to thank Editage ([www.editage.com](http://www.editage.com)) for English language editing.

**Author contributions** TS and SO wrote the main manuscript text. All authors reviewed the manuscript.

## Compliance with ethical standards

**Conflict of interest** The authors declare no conflict of interest.

**Open Access** This article is distributed under the terms of the Creative Commons Attribution 4.0 International License (<http://creativecommons.org/licenses/by/4.0/>), which permits unrestricted use, distribution, and reproduction in any medium, provided you give appropriate credit to the original author(s) and the source, provide a link to the Creative Commons license, and indicate if changes were made.

## References

1. Hille B (2001) Ion channels of excitable membranes, 3rd edn. Sinauer Associates Inc, Sunderland
2. Gonzalez C, Baez-Nieto D, Valencia I et al (2012) K<sup>+</sup> channels: function-structural overview. *Compr Physiol* 2:2087–2149
3. Oiki S (2015) Channel function reconstitution and re-animation: a single-channel strategy in the postcrystal age. *J Physiol* 593:2553–2573
4. Ishihara K (2019) New insights into K<sup>+</sup> dependences of the strong inward rectifier potassium channel Kir2.1. *J Physiol Sci* 69:S53
5. Bezanilla F, Armstrong CM (1972) Negative conductance caused by entry of sodium and cesium ions into the potassium channels of squid axons. *J Gen Physiol* 60:588–608
6. Doyle DA, Cabral JM, Pfuetzner RA et al (1998) The structure of the potassium channel: molecular basis of K<sup>+</sup> conduction and selectivity. *Science* 280:69–77
7. Noskov SY, Bernéche S, Roux B (2004) Control of ion selectivity in potassium channels by electrostatic and dynamic properties of carbonyl ligands. *Nature* 431:830–834
8. Neyton J (1988) Potassium blocks barium permeation through a calcium-activated potassium channel. *J Gen Physiol* 92:549–567
9. Piasta KN, Theobald DL, Miller C (2011) Potassium-selective block of barium permeation through single KcsA channels. *J Gen Physiol* 138:421–436
10. Zhou Y, MacKinnon R (2003) The occupancy of ions in the K<sup>+</sup> selectivity filter: charge balance and coupling of ion binding to a protein conformational change underlie high conduction rates. *J Mol Biol* 333:965–975
11. Liu S, Bian X, Lockless SW (2012) Preferential binding of K<sup>+</sup> ions in the selectivity filter at equilibrium explains high selectivity of K<sup>+</sup> channels. *J Gen Physiol* 140:671–679
12. Montoya E, Lourdes Renart M, Marcela Giudici A et al (2017) Differential binding of monovalent cations to KcsA: deciphering the mechanisms of potassium channel selectivity. *Biochimica et Biophysica Acta Biomembranes* 1859:779–788
13. Lockless SW, Zhou M, MacKinnon R (2007) Structural and thermodynamic properties of selective ion binding in a K<sup>+</sup> channel. *PLoS Biol* 5:e121
14. Hodgkin AL, Keynes RD (1955) The potassium permeability of a giant nerve fibre. *J Physiol* 128:61–88
15. Morais-Cabral JH, Zhou Y, MacKinnon R (2001) Energetic optimization of ion conduction rate by the K<sup>+</sup> selectivity filter. *Nature* 414:37–42
16. Zhou Y, Morais-Cabral JH, Kaufman A, MacKinnon R (2001) Chemistry of ion coordination and hydration revealed by a K<sup>+</sup> channel–Fab complex at 2.0 Å resolution. *Nature* 414:43–48
17. Berneche S, Roux B (2001) Energetics of ion conduction through the K<sup>+</sup> channel. *Nature* 414:73–77
18. Khalili-Araghi F, Tajkhorshid E, Schulten K (2006) Dynamics of K<sup>+</sup> ion conduction through Kv1.2. *Biophys J* 91:L72–L74
19. Jensen MØ, Borhani DW, Lindorff-Larsen K et al (2010) Principles of conduction and hydrophobic gating in K<sup>+</sup> channels. *Proc Natl Acad Sci USA* 107:5833–5838
20. Kratochvil HT, Carr JK, Matulef K et al (2016) Instantaneous ion configurations in the K<sup>+</sup> ion channel selectivity filter revealed by 2D IR spectroscopy. *Science* 353:1040–1044
21. Gordon D, Chung SH (2011) Permeation and block of the Kv1.2 channel examined using Brownian and molecular dynamics. *Biophys J* 101:2671–2678
22. Baştuğ T, Kuyucak S (2011) Comparative study of the energetics of ion permeation in Kv1.2 and KcsA potassium channels. *Biophys J* 100:629–636
23. Furini S, Domene C (2009) Atypical mechanism of conduction in potassium channels. *Proc Natl Acad Sci USA* 106:16074–16077
24. Flood E, Boiteux C, Lev B et al (2019) Atomistic simulations of membrane ion channel conduction, gating, and modulation. *Chem Rev* 119:7737–7832
25. Fowler PW, Abad E, Beckstein O, Sansom MSP (2013) Energetics of multi-ion conduction pathways in potassium ion channels. *J Chem Theory Comput* 9:5176–5189
26. Köpfer DA, Song C, Gruene T et al (2014) Ion permeation in K<sup>+</sup> channels occurs by direct Coulomb knock-on. *Science* 346:352–355
27. Ando H, Kuno M, Shimizu H et al (2005) Coupled K<sup>+</sup>-water flux through the HERG potassium channel measured by an osmotic pulse method. *J Gen Physiol* 126:529–538
28. Iwamoto M, Oiki S (2011) Counting ion and water molecules in a streaming file through the open-filter structure of the K channel. *J Neurosci* 31:12180–12188
29. Chang HK, Iwamoto M, Oiki S, Shieh RC (2015) Mechanism for attenuated outward conductance induced by mutations in the cytoplasmic pore of Kir2.1 channels. *Sci Rep* 5:18404
30. Furutani Y, Shimizu H, Asai Y et al (2012) ATR-FTIR spectroscopy revealing the different vibrational modes of the selectivity filter interacting with K<sup>+</sup> and Na<sup>+</sup> in the open and collapsed conformations of the KcsA potassium channel. *J Phys Chem Lett* 3:3806–3810
31. Levitt DG, Elias SR, Hautman JM (1978) Number of water molecules coupled to the transport of sodium, potassium and hydrogen ions via gramicidin, nonactin or valinomycin. *BBA-Biomembranes* 512:436–451
32. Rosenberg PA, Finkelstein A (1978) Interaction of ions and water in gramicidin A channels: streaming potentials across lipid bilayer membranes. *J Gen Physiol* 72:327–340
33. Oiki S, Iwamoto M, Sumikama T (2011) Cycle flux algebra for ion and water flux through the KcsA channel single-file pore links microscopic trajectories and macroscopic observables. *PLoS One* 6:e16578
34. Miller C (1982) Coupling of water and ion fluxes in a K<sup>+</sup>-selective channel of a sarcoplasmic reticulum. *Biophys J* 38:227–230
35. Alcayaga C, Cecchi X, Alvarez O, Latorre R (1989) Streaming potential measurements in Ca<sup>2+</sup>-activated K<sup>+</sup> channels from skeletal and smooth muscle. Coupling of ion and water fluxes. *Biophys J* 55:367–371
36. Sumikama T, Oiki S (2016) Digitalized K<sup>+</sup> Occupancy in the Nanocavity Holds and Releases Queues of K<sup>+</sup> in a Channel. *J Am Chem Soc* 138:10284–10292
37. Sumikama T, Oiki S (2018) An alternative permeation mechanism through the K<sup>+</sup> channel. *J Physiol Sci* 68:S68
38. Nimigean CM, Miller C (2002) Na<sup>+</sup> block and permeation in a K<sup>+</sup> channel of known structure. *J Gen Physiol* 120:323–335
39. LeMasurier M, Heginbotham L, Miller C (2001) KcsA: it's a potassium channel. *J Gen Physiol* 118:303–314
40. Iwamoto M, Oiki S (2018) Constitutive boost of a K<sup>+</sup> channel via inherent bilayer tension and a unique tension-dependent modality. *Proc Natl Acad Sci USA* 115:13117–13122
41. Chakrapani S, Cordero-Morales JF, Perozo E (2007) A quantitative description of KcsA gating II: single-channel currents. *J Gen Physiol* 130:479–496
42. Kasahara K, Shiota M, Kinoshita K (2013) Ion concentration-dependent ion conduction mechanism of a voltage-sensitive potassium channel. *PLoS One* 8:e56342
43. Delemotte L, Dehez F, Treptow W, Tarek M (2008) Modeling membranes under a transmembrane potential. *J Phys Chem B* 112:5547–5550
44. Jensen MØ, Jogini V, Eastwood MP, Shaw DE (2013) Atomic-level simulation of current–voltage relationships in single-file ion channels. *J Gen Physiol* 141:619–632

45. Sumino A, Sumikama T, Iwamoto M et al (2013) The open gate structure of the membrane-embedded KcsA potassium channel viewed from the cytoplasmic side. *Sci Rep* 3:1063
46. Iwamoto M, Oiki S (2013) Amphipathic antenna of an inward rectifier K<sup>+</sup> channel responds to changes in the inner membrane leaflet. *Proc Natl Acad Sci USA* 110:749–754
47. Blunck R, McGuire H, Hyde HC, Bezanilla F (2008) Fluorescence detection of the movement of single KcsA subunits reveals cooperativity. *Proc Natl Acad Sci USA* 105:20263–20268
48. Sumikama T, Saito S, Ohmine I (2013) Mechanism of ion permeation through a model channel: roles of energetic and entropic contributions. *J Chem Phys* 138:165106
49. Imai S, Osawa M, Takeuchi K, Shimada I (2010) Structural basis underlying the dual gate properties of KcsA. *Proc Natl Acad Sci USA* 107:6216–6221
50. Wylie BJ, Bhate MP, McDermott AE (2014) Transmembrane allosteric coupling of the gates in a potassium channel. *Proc Natl Acad Sci USA* 111:185–190
51. Furutani Y, Shimizu H, Asai Y et al (2015) Specific interactions between alkali metal cations and the KcsA channel studied using ATR-FTIR spectroscopy. *Biophys Physicobiol* 12:37–45
52. Shimizu H, Toyoshima C, Oiki S (2003) Interaction between tetraethylammonium and permeant cations at the inactivation gate of the HERG potassium channel. *Jpn J Physiol* 53:25–34
53. Tsitkov S, Pesenti T, Palacci H et al (2018) Queueing theory-based perspective of the kinetics of “channeled” enzyme cascade reactions. *ACS Catal* 8:10721–10731
54. Cookson NA, Mather WH, Danino T et al (2011) Queueing up for enzymatic processing: correlated signaling through coupled degradation. *Mol Syst Biol* 7:561
55. Xu Y, Bhate MS, McDermotto A (2017) Transmembrane allosteric energetics characterization for strong coupling between proton and potassium ion binding in the KcsA channel. *Proc Natl Acad Sci USA* 114:8788–8793
56. Bernèche S, Roux B (2000) Molecular dynamics of the KcsA K<sup>+</sup> channel in a bilayer membrane. *Biophys J* 78:2900–2917
57. Kopec W, Köpfer DA, Vickery ON et al (2018) Direct knock-on of desolvated ions governs strict ion selectivity in K<sup>+</sup> channels. *Nat Chem* 10:813–820
58. Berendsen HJC, Postma JPM, van Gunsteren WF et al (1984) Molecular dynamics with coupling to an external bath. *J Chem Phys* 81:3684–3690
59. Siu S, Vácha R, Jungwirth P, Böckmann R (2008) Biomolecular simulations of membranes: physical properties from different force fields. *J Chem Phys* 128:125103
60. Sumino A, Uchihashi T, Oiki S (2017) Oriented reconstitution of the full-length KcsA potassium channel in a lipid bilayer for AFM imaging. *J Phys Chem Lett* 8:785–793
61. Sumino A, Sumikama T, Uchihashi T, Oiki S (2019) High-speed AFM reveals accelerated binding of agitoxin-2 to a K<sup>+</sup> channel by induced fit. *Sci Adv* 5:eaax0495
62. Jorgensen W, Chandrasekhar J, Madura J et al (1983) Comparison of simple potential functions for simulating liquid water. *J Chem Phys* 79:926–935
63. Dang L (1995) Mechanism and thermodynamics of ion selectivity in aqueous solutions of 18-crown-6 ether: a molecular dynamics study. *J Am Chem Soc* 117:6954–6960
64. Cornell W, Cieplak P, Bayly CI et al (1995) A second generation force field for the simulation of proteins, nucleic acids, and organic molecules. *J Am Chem Soc* 117:5179–5197
65. Berendsen HJC, Grigera JR, Straatsma TP (1987) The missing term in effective pair potentials. *J Phys Chem* 91:6269–6271
66. Hornak V, Abel R, Okur A et al (2006) Comparison of multiple Amber force fields and development of improved protein backbone parameters. *Proteins* 65:712–725
67. Essmann U, Perera L, Berkowitz M (1995) A smooth particle mesh Ewald method. *J Chem Phys* 103:31–34
68. Ryckaert J, Ciccotti G, Berendsen HJC (1977) Numerical integration of the cartesian equations of motion of a system with constraints: molecular dynamics of n-alkanes. *J Comput Phys* 23:327–341
69. Case DA, Darden TA, Cheatham III TE et al (2010) AMBER 11. University of California, San Francisco
70. Delemotte L, Klein ML, Tarek M (2012) Molecular dynamics simulations of voltage-gated cation channels: insights on voltage-sensor domain function and modulation. *Front Pharmacol* 3:97
71. Contreras JE, Chen J, Lau AY et al (2010) Voltage profile along the permeation pathway of an open channel. *Biophys J* 99:2863–2869
72. Parzen E (1962) On estimation of a probability density function and mode. *Ann Mathem Stat* 33:1065–1076
73. Humphrey W, Dalke A, Schulten K (1996) VMD—visual molecular dynamics. *J Mol Graph* 14:33–38
74. Geng Y, Niu X, Magleby KL (2011) Low resistance, large dimension entrance to the inner cavity of BK channels determined by changing side-chain volume. *J Gener Physiol* 137:533–548

**Publisher's Note** Springer Nature remains neutral with regard to jurisdictional claims in published maps and institutional affiliations.